

Possible erosion mechanisms in snow avalanches

PETER GAUER, DIETER ISSLER*

Norwegian Geotechnical Institute, P.O. Box 3930, Ullevaal Stadion, N-0806 Oslo, Norway
E-mail: pg@ngi.no

ABSTRACT. Snow erosion and entrainment processes in avalanches are classified according to their mechanisms, the flow regimes in which they occur, and their spatial position within the avalanche. Simple, but process-specific, models are proposed for erosion by impacts, abrasion, plowing and blasting. On the basis of order-of-magnitude estimates, the first three mechanisms are clearly expected to be important. The fourth mechanism stipulates that the compaction of the snow cover ahead of the avalanche leads to the flow of escaping air just in front of the avalanche that may disrupt the snow cover and support formation of a saltation layer. The effects of this hypothetical mechanism resemble those of the plowing mechanism. All mechanisms depend strongly on the snow properties, but, with plausible parameter values, erosion rates at or above the experimentally found rates are obtained. The entrainment rate of an avalanche is most often limited by the shear stress needed to accelerate the eroded snow to avalanche speed.

1. INTRODUCTION

A few centuries ago, snow avalanches were depicted as ever growing snowballs rolling down mountainsides. One aspect of this naïve concept of avalanching has been vindicated by recent observations and measurements (Issler and others, unpublished; Sovilla and others, 2001): the entrainment of snow has now been recognized as a major factor in the dynamics of avalanches. It must be concluded that perhaps the majority of medium to large avalanches double or even triple their mass from release to runout; in the track, the moving mass may be more than five times the original mass (Sovilla and others, 2001). From measurements with profiling radars (Dufour and others, unpublished), erosion rates of $>200 \text{ kg m}^{-2} \text{ s}^{-1}$ have been inferred (Issler, 2003) during the very rapid removal of up to 1 m of fresh snow at the avalanche front, while they were found to be in the range $10\text{--}50 \text{ kg m}^{-2} \text{ s}^{-1}$ during episodes of more gradual entrainment in the head of dry snow avalanches.

It has long been recognized that entrainment has two aspects: One concerns the breaking up of the snow cover into particles (ranging in size from snow grains to large blocks); this process is the main focus of this paper and will be termed *erosion*. The *erosion speed*, w_e , is the velocity (measured in the direction perpendicular to the ground) at which the surface of the intact snow cover is lowered due to erosion. The other aspect is the *entrainment* of the eroded snow into the flow through acceleration and possibly mixing. The *entrainment rate*, $q_e = \rho_s \eta_e w_e$ ($\text{kg m}^{-2} \text{ s}^{-1}$), is the snow mass per unit time and unit area that is incorporated into the avalanche, where η_e is the fraction of the eroded snow that is eventually entrained. Entrainment distributes the avalanche momentum over a growing mass; the velocity diminishes unless there is sufficient net momentum gain from the gravitational and resistance forces, $m f_G$ and $m f_R$ (m is

the avalanching mass). To see this, the momentum equation for an avalanche entraining mass from a resting snowpack is $m \text{d}u_{\text{av}}/\text{d}t + u_{\text{av}} \text{d}m/\text{d}t = m f_G - m f_R$, or, rewritten as equation of motion, $\text{d}u_{\text{av}}/\text{d}t = f_G - f_R - f_E$. The effect on the avalanche of the entrained mass is that of a pseudo-force which causes a deceleration

$$f_E = \frac{u_{\text{av}} \text{d}m}{m \text{d}t} = \frac{\rho_s \eta_e w_e u_{\text{av}}}{\rho_{\text{av}} h_{\text{av}}} \quad (1)$$

Typical values for medium-size dry-snow avalanches on a 30° slope are $f_G = g \sin 30^\circ \approx 5 \text{ m s}^{-2}$, $u_{\text{av}} \approx 30 \text{ m s}^{-1}$, flow depth $h_{\text{av}} \approx 1 \text{ m}$, and ratio of avalanche density to snow-cover density $\rho_{\text{av}}/\rho_s \approx 1\text{--}2$. For $\eta_e w_e$ of $0.05\text{--}0.10 \text{ m s}^{-1}$, $f_E \approx (0.15\text{--}0.6) f_G$ is a substantial factor in the dynamics of the avalanche. In traditional avalanche models, these entrainment effects are subsumed in the velocity-dependent resistive forces and may contribute significantly to the wide scatter of back-calculated friction coefficients through the strong dependence of erosion and entrainment on topography, snow and avalanche properties.

This paper focuses on erosion mechanisms, but one should keep in mind that the entrainment rates that can be realized in snow avalanches are often limited, not by the work needed for eroding the snow, but by the large fraction of the available shear stress that is absorbed in the acceleration of the eroded snow.

The majority of dynamical (dense-flow) avalanche models that include snow entrainment do not model a specific entrainment process but add mass to the front of the avalanche at a rate specified by the user (Briukhanov and others, 1967; Brugnot and Pochat, 1981; Hungr, 1995; Sailer and others, 2002; Sovilla and Bartelt, 2002). A heuristic velocity-dependent entrainment function is used by Maeno and Nishimura (1987). Eglit (1983, 1998) assumes the entrainment rate to be proportional to the velocity, in analogy to the entrainment of ambient fluid in buoyant plumes or jets. Grigoryan and Ostroumov (1977) describe the erosion and entrainment process in terms of a compressive shock

*Present address: NaDesCoR, Promenade 129, CH-7260 Davos-Dorf, Switzerland.

front propagating through the snow cover underneath the avalanche body, inclined at an angle $\alpha = \arctan(w_e/u_{av})$ to the ground. The hydrostatic and dynamic pressures of the avalanche at the interface to the snow cover determine the compression of the eroded snow and the angle α , and thus the entrainment rate. For powder-snow avalanches, an entrainment function derived from flume experiments (Parker and others, 1987) has been used by Fukushima and Parker (1990) and in adapted form by Gauer (1995) to dynamically determine the mass increase of the flow.

The objective of this paper is to infer which erosion mechanisms are most likely to occur in real avalanches and therefore should be studied in more detail, both experimentally and theoretically. We build on concepts sketched in Issler and others (2000) and draw on work on wear and fatigue in solid mechanics and on river-bed erosion in hydraulics (see section 2). In section 5, we compare our order-of-magnitude estimates of the erosion speeds of the proposed mechanisms with the data from several measured avalanches.

2. EROSION PROCESSES IN OTHER PHENOMENA, AND SPECIFIC FEATURES OF EROSION IN SNOW AVALANCHES

Rabinowicz (1995) distinguishes four main types of wear, namely adhesive wear, abrasive wear, corrosive wear and surface fatigue wear, and a few special mechanisms. Among them, abrasive wear and possibly surface fatigue wear should be most relevant to erosion in avalanches. Impact erosion is generally believed to be the dominant mechanism in blowing and drifting snow, and has also been conjectured (Issler, 1998) to dominate in the saltation layer of powder-snow avalanches.

Abrasive wear occurs when hard asperities or particles slide over a softer surface, digging into it and plowing grooves. The snow particles in an avalanche undergo significant compression, by which their strength increases greatly; they are thus capable of indenting the usually much softer snow cover. Mears (1980, fig. 7) provides photographic evidence of abrasive processes at the base of the dense core of avalanches. Surface fatigue wear can be observed during repeated or continuous sliding over a surface. The sliding induces surface or subsurface cracks which eventually result in the break-up of the surface. This mechanism is often observed during springtime, when small avalanches break loose and start to erode the whole snowpack. The photograph mentioned above also shows a crack from the sliding surface deep into the snowpack. Impact erosion occurs when particles impinge on the snow-cover surface and, while moving along the surface, abrade material or initiate cracking of the surface. In section 3, we present models for the abrasion and impact erosion in avalanches.

Three main erosion mechanisms are discussed in the fluvial hydraulics literature (see, e.g., Partheniades, 1965; Mehta, 1991; Zreik and others, 1998): Gradual erosion of single particles from the surface occurs already at shear stresses an order of magnitude smaller than the mechanical shear strength of the bed. (In non-cohesive granular beds, surface erosion is also observed to set in at shear stresses about one order of magnitude lower than the mechanical shear strength.) Under stresses comparable to the shear strength, entire chunks of material are ripped off the bed following failure along a deeply embedded plane (mass erosion).

Finally, waves cause cyclic loading/unloading and shear stress; this may lead to fluidization of the surface layer and subsequent entrainment and mixing (Mehta, 1991).

The mechanisms observed in fluvial systems need not be directly relevant to (dense) snow avalanches because of the low density of air and the overwhelming effect of particle interactions with the snow cover. Nevertheless, there is presently an indication that mass erosion may also occur in snow avalanches (see section 5), and fluidization of the snowpack immediately in front of the avalanche (due to excess pore pressure generated during snow compression) or inside a dilute head (as a consequence of under-pressure at the snow-cover surface) is considered in section 4.

In all erosion processes, an important factor is the strength of the eroded material. The snow strength generally grows substantially with depth as the density increases (except for weak layers) and will usually exceed the avalanche stress at some point. It is indeed often observed that erosion proceeds only to the interface between the fresh snow and the old snowpack (Issler and others, unpublished; Sovilla and others, 2001). The strength of snow shows a varying strain-rate dependency. Abele and Gow (1975) performed strength tests under rapid uniaxial loading in which the strain rates were close to those expected in the case of an avalanche. The stress-strain curves indicate an initial phase of plastic behavior, when the major principal stress exceeds the yield strength, Y . During the plastic collapse, the stress stays approximately constant until the strain reaches the critical plastic strain, ε_m , beyond which rapid strain hardening occurs. Based on these tests, the following relations between the yield strength under compression, Y (in kPa), and the snow-cover density, ρ_s (in kg m^{-3}), and between ε_m and ρ_s , are derived to characterize the snow-cover properties:

$$Y = 2.1 \times 10^{\frac{\rho_s - 100}{150}} \quad (2)$$

$$\varepsilon_m \approx \max(-7.0 \times 10^{-4} \rho_s + 0.268, 0). \quad (3)$$

Some inferences can immediately be drawn from these properties: (i) the exponential dependence of snow strength on snow density leads to a strong variability of erosion speeds; (ii) the yield strength Y can be used in first estimates of erosion rates, but will lead to overestimates; and (iii) strain hardening will limit the densification to values similar in large, fast avalanches to those found in smaller ones, despite significantly higher stresses.

3. EROSION BY DIRECT PARTICLE-PARTICLE INTERACTION

Measurements with profiling radar (see Fig. 1) show relatively long episodes with gradual erosion at moderate rates, indicating the importance of snow erosion due to particles impinging on the snow surface within the saltation layer of avalanches. Each impact partly leads to a densification of the snowpack, partly to loosening of snow and its entrainment by the ambient flow. The impacting particle itself may rebound from the surface or penetrate it and get stuck. The particle sizes range from approximately 0.25 mm to a few decimeters.

At the base of the dense avalanche core, the particles are in continuous contact and slide over one another. Hard

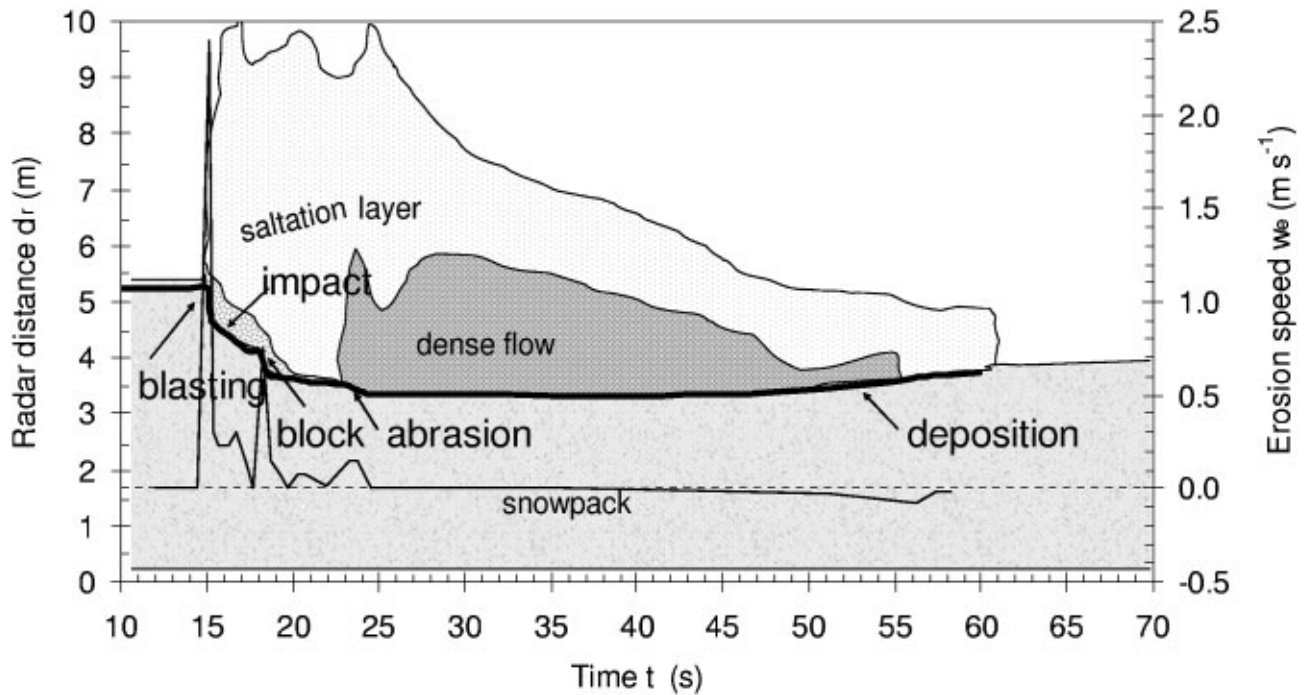


Fig. 1. Radar distance of the snow surface from ground vs time (thick line), and the corresponding erosion speed (thin line). The association to the different flow regimes is based on the radar echo intensity. Vallée de la Sionne (Switzerland) test site, radar A2, event of 25 February 1999 (derived from radar plot in Dufour and others (unpublished)).

particles will plow grooves in the snowpack under their own weight and the overburden load. The snow cover is partly compacted and partly loosened and entrained by the avalanche. This process is commonly known as abrasion. In the following, we present a simple model for impact erosion and its adaptation to the abrasion mechanism.

3.1. Erosion due to particle impact

According to Johnson (2001, ch. 11), the impact of snow particles on the snowpack during an avalanche can cause the whole range from elastic–plastic over fully plastic to extensive plastic displacement (flow) and the onset of hydrodynamic behavior. For a first estimate of potential impact erosion speeds, we assume fully plastic impacts. We treat the avalanche particle as a rigid sphere with radius $r (= d_p/2)$, density ρ_p and mass $m_p = \rho_p V_p$ and the snowpack as a porous, rigid and perfectly plastic material with compressive yield strength Y . During impact the latter decelerates the particle and deflects it upwards (provided the particle is not completely submerged in the snow cover). If the impact angle α (measured from the x axis and thus negative) is sufficiently small, the particle will not be stopped completely but will leave the snow cover again.

The equations of motion for the impinging particle read (neglecting aerodynamic drag):

$$\ddot{x} = g \sin \phi - \frac{P_L}{m_p} [\sin(\alpha + \beta) + \mu \cos(\alpha + \beta)] \quad (4)$$

$$\ddot{z} = -g \cos \phi + \frac{P_L}{m_p} [\cos(\alpha + \beta) - \mu \sin(\alpha + \beta)], \quad (5)$$

where ϕ is the slope angle, $P_L = p_d A_e$ is the force due to the plastic flow pressure acting in the line of penetrating motion and μP_L is the contribution of the Coulomb friction tangential to the motion. A_e is the projection of the instantaneous

contact area onto the plane defined by \overline{AB} and the y axis (see Fig. 2).

The plastic flow pressure is approximated as $p_d \approx c_p Y$. For solids, $c_p \approx 3$ in the fully plastic stage. c_p is close to unity in porous media in the fully plastic stage and for small indentations. With increasing indentation, c_p increases to about 3, reflecting strain hardening. Thus, snow as a porous medium might have a c_p similar to that of foams, for which Wilesa and others (1975) give

$$c_p = \left(1 - \frac{[\overline{AB}/(4r\varepsilon_m)]^3}{\{1 + [\overline{AB}/(4r\varepsilon_m)]^2\}^{3/2}} \right)^{-1} \quad (6)$$

for the case of an indenting sphere. The critical strain ε_m is given in Equation (3). Further hardening of the snowpack due to dynamic flow effects is disregarded. The total volume V_e of the impact crater is

$$V_e = \int_0^{t_i} \mathbf{A}(t) \cdot \mathbf{U}_p(t) dt, \quad (7)$$

where $\mathbf{A}(t)$ is the penetrating cross-sectional area perpendicular to the line of motion, $\mathbf{U}_p(t)$ is the instantaneous

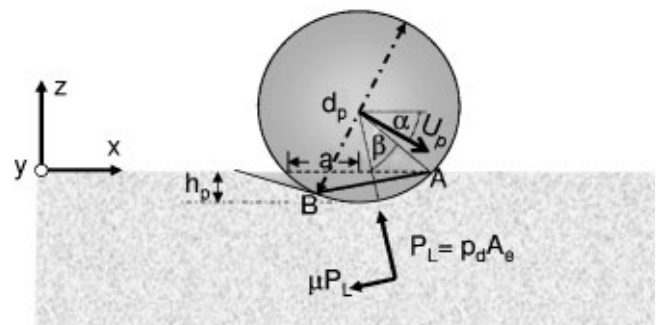


Fig. 2. Rigid snow particle impacting onto the plastic snowpack. Adapted from Rickerby and Macmillan (1980).

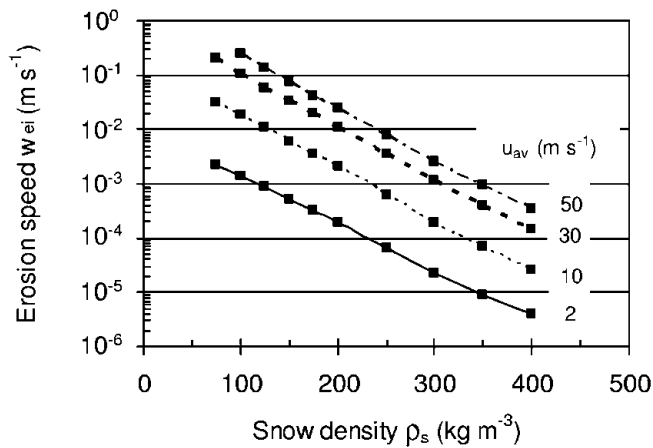


Fig. 3. Impact erosion speed vs snow density, with the avalanche velocity as parameter; $\rho_{av} = 10 \text{ kg m}^{-3}$; $d_p = 0.25 \text{ mm}$; $\phi = 0^\circ$.

velocity of the particle, and t_i is the duration of the impact. For a full description of the geometric relations we refer to Rickerby and Macmillan (1980). To calculate the total crater volume, Equations (4) and (5) are solved numerically. The impact angle α_i , needed as an initial condition, depends on the ratio between terminal velocity of the particle, W_f , and avalanche velocity and might also be influenced by the turbulence. The number of particle impacts per unit time and unit area, N_i , can be approximated by

$$N_i \approx \frac{cW_f \cos \phi}{2V_p}; \quad (8)$$

here $c/2$ is the volume concentration of particles in downward motion. The erosion speed due to particle impacts can now be written as

$$w_{ei} = N_i V_e. \quad (9)$$

Each particle impact causes a momentum transfer $m_p(U_{p1\parallel} - U_{p0\parallel})$ from the avalanche to the snowpack even without entrainment, where $U_{p0\parallel}$ and $U_{p1\parallel}$ are the mean particle velocities parallel to the surface before and after the impact, respectively. Some of this momentum is returned to the flow by the fraction η_{ei} of ejected particles (with mean initial velocity $U_{pe\parallel}$) that are eventually entrained by the avalanche. The difference of the two contributions is the so-called grain-borne shear stress:

$$\tau_g = N_i m_p (U_{p1\parallel} - U_{p0\parallel}) + \eta_{ei} w_{ei} \rho_s U_{pe\parallel}. \quad (10)$$

Figures 3 and 4 plot the calculated impact erosion speeds and grain-borne shear stresses due to particle impact vs the snow density. The essentially exponential dependence on the snow density is a result of Equation (2). Another controlling factor is the impact angle. The erosion speed grows with increasing impact angle and thus with particle size because larger particles have a higher fall velocity W_f and thus tend to impact under a steeper angle. The dependence on the impact angle also influences the relationship between avalanche speed and erosion speed because the impact angle decreases with increasing avalanche speed. If the impact angle is artificially kept constant in the simulations, $w_{ie} \propto u_{av}^n$, with $n > 2$, but if it is made to vary according to $\alpha_i = -\arctan(W_f \cos \phi / u_{av})$, one finds $1 < n < 2$ (for $d_p = 25 \text{ mm}$, $n \approx 1.5$). Note that the growth of the erosion speed with increasing impact angle is sharply limited by the

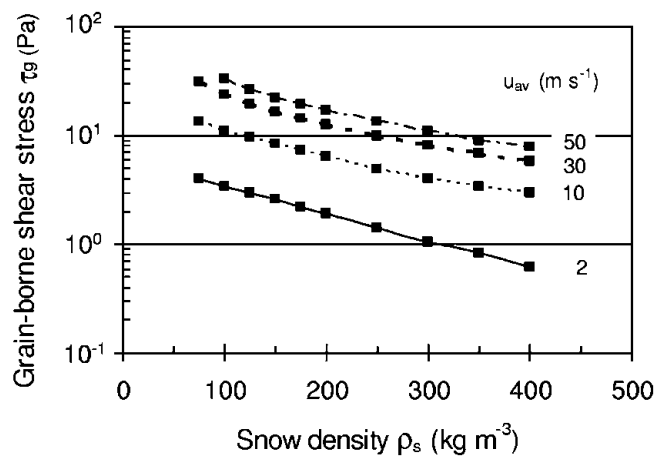


Fig. 4. Shear stress due to momentum loss of impacting particles vs snow density, with the avalanche velocity as parameter; $\rho_{av} = 10 \text{ kg m}^{-3}$; $d_p = 0.25 \text{ mm}$; $\phi = 0^\circ$; $U_{pe} = 0$.

maximum angle (depending on the impact velocity) beyond which the particle is absorbed in the snowpack.

3.2. Abrasion

The methods developed for impact erosion may also be applied to estimate the abrasion speed. Consider a snow particle indenting the snowpack and sliding parallel to the surface ($\alpha = 0$). The particle equations of motion (4) and (5) are supplemented with an overburden load L and the traction exerted by the avalanche:

$$\ddot{x} = \left(g + \frac{L}{m_p} \right) \sin \phi - \frac{P_L}{m_p} (\sin \beta + \mu \cos \beta) + \frac{F_D}{m_p}, \quad (11)$$

$$\ddot{z} = - \left(g + \frac{L}{m_p} \right) \cos \phi + \frac{P_L}{m_p} (\cos \beta - \mu \sin \beta) + \frac{F_D}{m_p}. \quad (12)$$

L is determined by the effective pressure transferred through the particle lattice within the avalanche. We assume that each snow block at the interface carries the load $L = \rho_{av} g h_{av} / N_b$, with N_b the number of blocks per unit footprint area. For simplicity, the traction is expressed as a drag: $F_D \approx (C_D/2) \rho_{av} \pi r^2 |u_{av} - U_p| (u_{av} - U_p)$, with U_p the velocity of the sliding particle. The drag coefficient, C_D , depends on the flow regime.

In the present case of surface-parallel sliding, the left-hand side of Equation (12) vanishes, and the plastic-flow pressure times the z component of \mathbf{A}_e balances the load due to the particle and its overburden. At the same time the plastic-flow pressure times the x component of \mathbf{A}_e acts as the retarding force in Equation (11). Summing the retarding forces over all N_b blocks gives the frictional stress, τ_f , acting at the bottom of the avalanche. As long as the slope-parallel component of gravity and the drag force acting on the blocks together equal or exceed the retarding force, the blocks plow through the snow cover and erode it. If the retarding force exceeds the driving forces, the blocks decelerate and the drag force grows accordingly; however, if the maximum drag force is insufficient to overcome the retarding force on the block, deposition begins. The total shear stress at the interface between the plowing blocks and the overriding layer of the avalanche also includes the drag

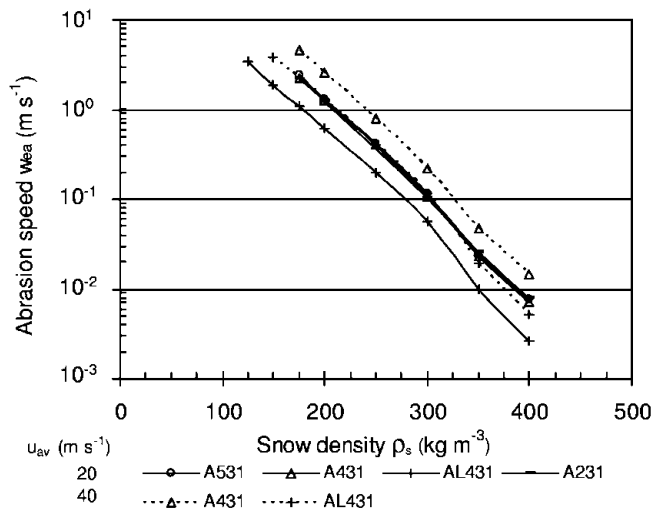


Fig. 5. Abrasion speed vs density of the snowpack for the parameter sets listed in Table 1. Avalanche velocity is treated as an externally prescribed constant; erosion rates in real avalanches would be significantly lower.

forces on the eroded snow that accelerate it to the avalanche velocity during mixing.

The material eroded by one block per unit time is proportional to the penetrating cross-sectional area, A , perpendicular to the flow direction and the mean velocity of the block, \bar{U}_p . Hence, the erosion speed due to abrasion is

$$w_{ea} = N_b A \bar{U}_p. \tag{13}$$

Figures 5 and 6 show the simulated abrasion rates and frictional stresses, τ_f , as functions of the snow-cover density. The parameters used are given in Table 1. The avalanche speed, u_{av} , is not treated as a dynamical variable here but as an externally prescribed constant. The determining factors for the abrasion speed are the snow density (via the exponential dependence of strength on density) and the effective overburden of the particles at the base. There is only a weak particle-size dependence. The shear stress between the plowing particles and the snow cover diminishes with increasing snow strength because the grooves strongly diminish in depth and the slope-parallel component of the resistance force at the interface becomes rather small while the slope-perpendicular component remains constant.

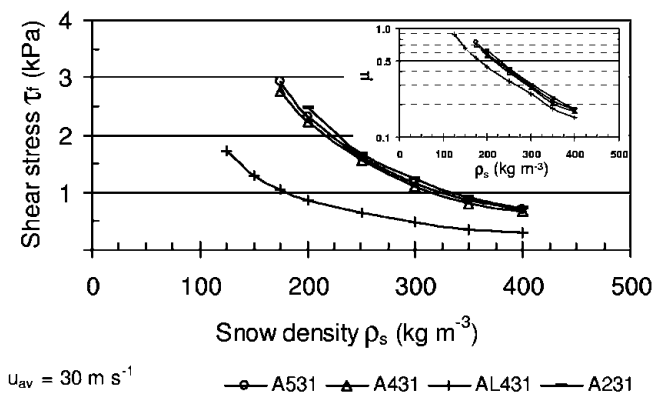


Fig. 6. Shear (frictional) stress due to abrasion vs snow density for the parameter sets listed in Table 1. The inset shows the corresponding friction coefficient μ (ratio of shear stress vs normal stress).

Table 1. Compilation of parameters used in the simulation of abrasion

Simulation	d_p mm	ρ_p kg m^{-3}	ρ_{av} kg m^{-3}	h_{av} m	μ
A531	100	450	200	2	0.1
A431	10	500	200	2	0.1
A231	1	750	200	2	0.1
AL431	10	500	200	1	0.1

Notes: d_p : particle diameter; ρ_p : particle density; ρ_{av} : avalanche density; h_{av} : avalanche flow depth; μ : apparent dry-friction coefficient of the particle; slope angle $\phi = 0^\circ$.

4. EROSION MECHANISMS AT THE AVALANCHE FRONT

In avalanches, aerodynamic entrainment of the snow cover might play a role just in front of the avalanche where ambient air is rapidly displaced by the approaching avalanche. This phase may last about 1–2 s in a developed powder-snow avalanche. Estimates using the widely used excess shear-stress approach for the erosion speed (see, e.g., Anderson and Haff, 1991) show that the erosion speeds are in the range 0–0.003 m s^{-1} under the most favorable assumptions, and are thus negligible.

4.1. Fluidization of the snowpack by pore-air displacement

Excess pore-water pressure can fluidize river beds and thus significantly affect the erosion process (Simon and Collison, 2001). An air-pressure gradient can also arise at the front of snow avalanches where (i) the rapid flow of the dilute snow–air mixture causes a pressure drop above the snow cover, or (ii) the snow cover is rapidly compacted by the avalanche and pore air tries to escape through the undisturbed snow cover.

The first-mentioned situation is expected to occur during the passage of a dilute avalanche front, in which the pressure drop is $\Delta p \sim (1/2)\rho_{af}u_{af}^2$. ρ_{af} and u_{af} are the density and avalanche speed at the front. This pressure drop has been measured in experiments with ping-pong balls (McElwaine and Nishimura, 2001). Due to this drop, a pressure difference between the interior of the snowpack and the surface builds up during a short but finite time, t_f , of front passage, persists for a while and vanishes gradually. A given volume of snow becomes fluidized when the force due to the flow of escaping air exactly balances the net force due to gravity and strength. Taking for simplicity a hexahedral control volume with length l ($\sim u_{av}t_f$) and width w , and assuming tensile strength Y_t and shear strength Y_s , fluidization should occur to a depth

$$d_e = \frac{\Delta p(d_e, t/t_f) - Y_t}{\rho g \cos \phi + 2 \frac{l+w}{lw} Y_s}. \tag{14}$$

This is an implicit equation for d_e , showing that simultaneous fluidization of as large an area as the pressure gradient permits is most advantageous. The effectiveness in

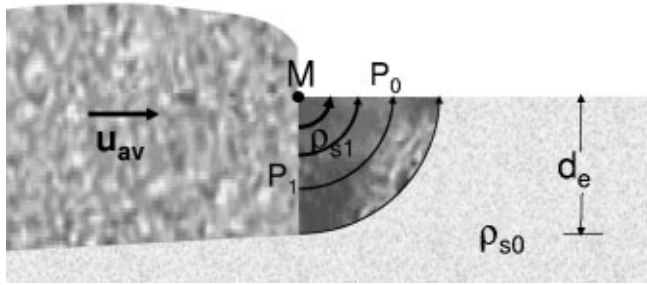


Fig. 7. Schematic representation of airflow through the snow-pack ahead of the moving avalanche.

fluidizing the top of the snow cover moreover depends crucially on the ratio of the build-up time, t_f , to the pressure relaxation time, $t_r (\approx \nu d_e^2 / (kRT))$, where k is the intrinsic permeability of the snowpack, ν the kinematic viscosity of air, R the specific gas constant of air and T the temperature). The erosion speed w_{ef} is on the order of d_e / t_f . At present, it is unclear whether fluidization due to pressure drop can occur at the front of the saltation layer, as no firm data from snow avalanches are available. Estimates of the pressure drop required for fluidizing snow covers with density $75\text{--}200 \text{ kg m}^{-3}$ yield velocities in the range $20\text{--}75 \text{ m s}^{-1}$ if a (powder-snow) avalanche density of 5 kg m^{-3} is assumed. However, even if complete fluidization is not reached, this mechanism will contribute to the weakening and destruction of the snowpack and is a candidate mechanism for the blast-like erosion seen in Figure 1.

The second mechanism involves rapid (adiabatic) compression of the snow cover by the weight of the avalanche flowing over it or plowing into it. Snow compaction from a density ρ_{s0} to ρ_{s1} leads to a pore-air pressure rise

$$\Delta p = p_0 \left[\left(\frac{\rho_i - \rho_{s0}}{\rho_i - \rho_{s1}} \right)^{1.4} - 1 \right], \quad (15)$$

where p_0 is atmospheric pressure and ρ_i the density of ice. Some of the pore air is pressed at high speed through the snow cover ahead of the avalanche front in a narrow zone, the length of which is comparable to the erosion depth at the front, i.e. a few meters or probably less. The pressure gradient is non-uniform and depends strongly on the geometry of the avalanche head; it should be greatest where the avalanche front intersects the snow cover. Depending on the snow strength and the pressure difference Δp , there is a limiting depth d_e below which the pressure gradient is too weak to fluidize the snow cover.

To illustrate the mechanism, we approximate the streamlines ahead of the (slope-perpendicular) avalanche front by concentric quarter-circles about the intersection of the avalanche front and the snow cover (point M in Fig. 7). From the balance of the moments of the gravity, pressure and shear forces, the erosion depth is estimated as

$$d_e = \frac{3}{2} \frac{\Delta p - \pi Y_s}{\rho_s g (\cos\phi - \sin\phi)}. \quad (16)$$

The mean erosion speed according to Equation (16) is equal to u_{av} . However, this estimate implies that the penetration depth of the avalanche front adapts to potential erosion depth. For a more comprehensive approach see the discussion in section 6 and the following subsection.

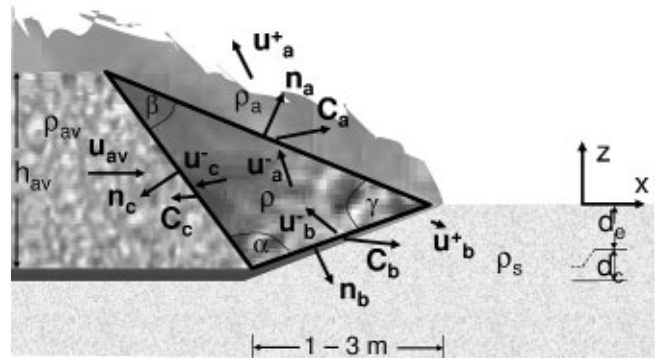


Fig. 8. Schematic representation of the head region of a dense-flow avalanche plowing through the snowpack. The triangle represents the control volume for which the jump conditions have to be solved d_e indicates the erosion depth and d_c the part of the snowpack that will be compacted by the avalanche.

4.2. Plowing

It has been observed that the front of dense-flow avalanches plows through the snowpack and entrains large quantities of snow thereby, even at moderate velocities. Such plowing implies that the snowpack undergoes strong, rapid shearing and compaction just ahead of the avalanche. We expect the length of this area to be about 1–3 m. Part of the snow cover is compacted and overflowed by the avalanche (which may ultimately abrade it). The upper part of the plowed snow-cover layer is pushed onto the avalanche front where it may pile up or be advected to the avalanche body, possibly being comminuted and suspended.

In order to describe the compaction and erosion process, consider a prismatic control volume bounded by three surfaces (see Fig. 8). Surface b forms the shear surface, surface c is the boundary towards the avalanche, and surface a forms the boundary to the airflow above. Across each of these surfaces, the jump conditions for mass and momentum must be fulfilled:

$$[[\rho_r(\mathbf{u}_r - \mathbf{C}_r) \cdot \mathbf{n}_r]] = 0, \quad (17)$$

$$[[\rho_r \mathbf{u}_r(\mathbf{u}_r - \mathbf{C}_r) \cdot \mathbf{n}_r]] - [[\mathbf{t}_r \cdot \mathbf{n}_r]] = 0, \quad (18)$$

where r indicates the surfaces a , b and c , respectively. \mathbf{C}_r is the velocity of the (non-material) surfaces, and $\mathbf{t}_r \cdot \mathbf{n}_r$ is the normal stress onto the respective surface. The erosion depth d_e is strongly influenced by the normal stresses at the shear plane b . Here, the determining quantities are the compressibility of the snowpack and the overburden load from the avalanche head. Across the interface a , excess pore-air pressure generated by the compaction may play a role in supporting the development of the saltation layer on the upper surface of the dense core. Along the surface c , dispersive pressure may come into play. Further study of this problem is needed in order to obtain approximate solutions that can be compared to measurements.

Two entrainment models have been published that contain elements of the analysis suggested above: Grigorian and Ostroumov (1977) consider only one jump surface underneath the dense core; the entire entrainment is into the dense flow. The model by Sailer and others (2002) distinguishes between entrainment into the dense flow and into the suspension layer, but the jump conditions for the

momentum are not evaluated and hence neither the erosion depth nor the ratio between entrainment at the bottom and at the top can be determined dynamically in their model.

5. COMPARISON WITH EXPERIMENTS AND FIELD OBSERVATIONS

Figure 1 shows the time evolution of the snow-cover and flow depths as well as the erosion speed for the giant avalanche of 25 February 1999 at the Vallée de la Sionne test site in Switzerland. The plot is derived from data from a profiling radar located in the upper track (Dufour and others, unpublished). The association of different areas in the avalanche with different flow regimes is based on the radar echo intensity; the suspension layer is invisible to the frequency-modulated continuous wave radar. The preliminary analysis of simultaneous Doppler radar measurements indicates velocities on the order of 50 m s^{-1} at that point. The snow density was in the range $170\text{--}300 \text{ kg m}^{-3}$. Approximately 0.7 m of snow are eroded virtually instantaneously at the leading front of the saltation layer, corresponding to an erosion speed of about 2.5 m s^{-1} . In the following 5 s, erosion is more gradual, with erosion speeds decreasing from 0.25 m s^{-1} to near zero. During this time, an approximately 0.5 m thick layer of higher echo intensity can be seen, indicating a higher density and/or larger block size than in the upper reaches of the saltation layer. The second peak at 18–19 s in the erosion speed curve is tentatively interpreted as a snow block ripped out of a stronger layer. After that, the average erosion speed is about 0.05 m s^{-1} and no denser bottom layer is found until the dense core arrives. During the first second of its passage, the erosion speed jumps back to about 0.15 m s^{-1} , but no further erosion is observed afterwards. Snow deposition takes place during the last 10 s of the passage of the dense part. Over the entire avalanche passage (lasting about 45 s), the mean erosion speed is 0.05 m s^{-1} .

This recording suggests that both a very rapid plowing or fluidization mechanism at the front and gradual, impact-driven erosion in a relatively dilute avalanche head (tentatively identified as the saltation layer, with an estimated density around 100 kg m^{-3}) may occur in large dry-snow avalanches. Additional radar recordings from the same site lend support to this conclusion (Dufour and others, unpublished), although the ratio of the masses entrained by the different mechanisms varies considerably. A much more detailed analysis combining data from different sensors and comprising all avalanches measured at the test site is needed in order to correlate these differences with the dynamics of the avalanches.

For a number of small avalanches, Sovilla and others (2001) carried out a systematic study of the mass balance at the avalanche test site Monte Pizzac at Arabba in the Dolomites, Italy. Additional information on these avalanches is contained in Somnavilla and Sovilla (1998) and Sovilla and Bartelt (2002). Perhaps the best described of these events is that of 21 December 1997. The most reliable data for the estimation of the erosion speed are given at pole 1 (position A) at 2024 m a.s.l. For the event of 5 March 1999, the width of the track swept by the avalanche had to be estimated. Both events are classified as dry dense-flow avalanches. Table 2 summarizes the measurements for these two events at pole 1 and gives the calculated mean erosion speed and

Table 2. Compilation of measurements at pole 1 in the Monte Pizzac path (after Somnavilla and Sovilla, 1998; Sovilla and others, 2001; Sovilla and Bartelt, 2002), and calculated erosion speeds and avalanche densities at the same point

	Event	
	27 Dec. 1997	5 Mar. 1999
<i>Measurements</i>		
Velocity (m s^{-1})	24	19
Time of passage (s)	9.25	12.7
Mean flow depth (m)	1	1
Total mass (t)	365	200
Entrained mass/area (kg m^{-2})	150	–
Pressure (kPa) at 1.0 and 1.8 m	80 and 50	–
Snow-cover density (kg m^{-3})	140–290	160–320
<i>Inferred avalanche parameters</i>		
Length (m)	220	220
Width (m)	13.5	≈ 10
Erosion rate (mean) ($\text{kg m}^{-2} \text{ s}^{-1}$)	17.1	8.2
Erosion speed (mean) (m s^{-1})	0.075	0.034
Avalanche density (kg m^{-3})	120	90

the inferred avalanche density. The avalanche density of the 21 December 1997 event, inferred from the volume and mass estimates, compares quite well with the reported pressures if $p_{\text{impact}} \approx \rho_{\text{av}} u_{\text{av}}^2$ is assumed for the 10 cm diameter load cells used at Monte Pizzac. The pressure sensor at 1 m above ground was just above the snow surface and thus should reflect the pressure in the flowing part of the avalanche.

Field observations on a small to medium avalanche in Seewis, Grisons, Switzerland (Issler and others, unpublished), where the powder-snow part separated from the dense flow at a sharp turn of the gully, allow the erosion speed within the saltation layer to be estimated, provided several reasonable but not directly verifiable assumptions are made. The new-snow layer had a depth of 0.7–1 m and a density of approximately 120 kg m^{-3} . Tracers (mostly fir needles and twigs) in two snow pits excavated at different locations showed that the new-snow layer was completely eroded at one location and reduced to 10–20 cm at the other; it remains an open question whether old snow was eroded at the location of the first snow pit.

In the first pit location, the deposit depth measured 30–50 cm and the largest particles had diameters up to 40 cm; in the second, the deposit depth measured 5–10 cm and the largest snow particles were the size of an egg. Depending on the assumed deposit density (measurements are not available), mass deposition from the tail of the powder-snow avalanche was comparable to the erosion in the head at snow pit 1, but clearly less at pit 2 despite the less violent erosion there. This can be explained by the location of the snow pits: pit 2 is close to the side of the path, but in fairly steep terrain, so the velocities were generally lower than in the center of the track, but even the dilute tail is expected not to decelerate. Pit 1, in contrast, is in the center of the powder-snow avalanche path, but further downstream in less steep terrain shortly after the cloud had to climb about 20 m along the steep side-wall of the gully turn.

From numerical simulations, the front velocity and the length of the powder-snow avalanche are estimated as 35 m s^{-1} and 300 m, respectively. If we further assume that erosion occurred only in the front half and deposition only

Table 3. Simulated erosion speeds in m s^{-1} for the four events described in the text

Mechanism	Event			
	VdlS 25 Feb. 1999	Monte Pizzac 27 Dec. 1997	5 Mar. 1999	Seewis 11 Jan. 1995
Fluidization	13.0 (1.34 m)	–	–	9.1 (1.0 m)
Impact	0.23 (SL)	0.08	0.02	0.03–0.06
Plowing	?	?	?	–
Abrasion	0.16 (DF)	0.06	0.02	–

Notes: The assumptions for the density of the Vallée de la Sionne avalanche (VdlS) of 25 February 1999 are: leading part of the saltation layer (SL), 90 kg m^{-3} ; dense part (DF), 200 kg m^{-3} . For the 11 January 1995 avalanche near Seewis, a density of $5\text{--}10 \text{ kg m}^{-3}$ was assumed for the powder-snow part. Values in parentheses indicate the contribution of the respective mechanism to the total erosion depth.

in the tail half, the mean erosion speed was around 0.2 m s^{-1} at pit 1 and 0.1 m s^{-1} at pit 2. Similar erosion speeds are inferred in the run-up area of the large 10 February 1999 avalanche at Vallée de la Sionne where almost the entire snowpack of 2 m depth was eroded near the shelter (Dufour and others, 1999) and the deposit depth varied from 0.2 to 2 m over distances of 10–20 m.

Table 3 summarizes the predicted contributions to the erosion speeds from fluidization, impact erosion and abrasion in the four avalanches discussed in section 5. We have not developed a dynamical model for the plowing mechanism yet, so no predictions can be made; it is very likely, however, that the powder-snow part of the Seewis avalanche did not erode by plowing. Considering the uncertainty and incompleteness of the measurements, the agreement between the measured (or inferred) entrainment speeds and the model predictions is encouraging. For the two events at Monte Pizzac, simulated abrasion and impact erosion speeds are similar; it is quite conceivable that the front of those avalanches was more dilute than the main body and that impact erosion dominated in the front, abrasion in the body. For the 25 February 1999 event at Vallée de la Sionne, the maximum impact erosion speed is approximately 1.3 m s^{-1} for reasonable assumptions. This is about half the erosion speed inferred from the radar measurement; thus the observed erosion during the front passage cannot be explained by impact erosion alone. The field observations from Seewis also indicate that either our estimates are too low, or an additional mechanism is operating; fluidization is an obvious candidate, but more work is needed to make testable predictions.

6. DISCUSSION AND CONCLUSIONS

In this exploratory study, five potential mechanisms for erosion in snow avalanches have been identified. Surface fatigue wear may occasionally occur as localized mobilization of a deeper layer in the snowpack, but may be neglected at present. Impact erosion and abrasion have many common aspects, but the conditions for their occurrence are quite different, especially with regard to the avalanche density. Neither mechanism has been observed directly, but grooves and impact holes have been seen in several cases. Under the mechanical conditions in the saltation layer (relatively low density, large blocks, high

velocities), impact erosion appears quite unavoidable. It is conceivable that the saltation layer often erodes the snow cover down to a hard layer of old snow on which the snow blocks in the bottom layer of the dense core are quickly comminuted and abrasion becomes negligible.

The plowing and fluidization mechanisms may be more intimately connected than our crude and incomplete treatment in section 4 suggests; perhaps they should be regarded as two aspects of a single phenomenon. After all, plowing represents the most efficient mechanism for generating a strong pressure gradient in the snow cover immediately in front of the avalanche. Both processes are subjected to feedback mechanisms that require further study and need to be formulated mathematically.

We wish to emphasize two points: First, abrasion, impact erosion, plowing and fluidization all have the potential to contribute strongly to entrainment under certain conditions, and they do so in different locations of the avalanche. Thus they all need to be studied further and eventually incorporated into a comprehensive entrainment/deposition model for avalanche simulation codes. Second, when soft fresh snow is abundant, i.e. under the conditions that favor large, catastrophic mixed avalanches, acceleration of the eroded snow and mixing with the avalanche is the limiting factor. The resistance of the snow cover against erosion becomes important if the snow cover is old and/or relatively warm and humid.

Further progress in the modeling of erosion and entrainment requires not only dedicated theoretical studies of the candidate mechanisms, but also a series of experiments that shed light on the unresolved questions. Some of the experiments are best carried out in the laboratory (or on an outdoor chute); others require a well-equipped full-size test site. In the authors' opinion, the most promising approaches are:

High-resolution close-up videos of avalanches in (natural) chutes, taken from the side, will help distinguish between different erosion mechanisms.

Pore pressure measurements. Such measurements have been carried out at the bottom of debris flows (Iverson, 1997) and should also be feasible in snow avalanches, preferably at several levels on an instrument support structure.

Particle-impact experiments with snowballs of various sizes and hardness, different velocities, and impact angles onto a snow surface of known properties.

Direct measurements of the erosion rate. In real avalanches, the erosion rate is usually limited by the large force needed to accelerate the eroded snow. It might be possible to design laboratory experiments in which the "avalanche" body is pulled across the snow cover at constant speed, irrespective of the entrainment rate and the force needed.

Tracer experiments to determine the degree of mixing of eroded snow into the avalanche. In chutes or small avalanche tracks, various kinds of tracers could be deployed in different locations along the track and at various depths in the snow cover before the avalanche release.

Measurement of velocity profiles and density.

More than one erosion mechanism has to be included in a satisfactory avalanche model: the measurements available so far indicate clearly that entrainment takes place both at

the front and along the bottom of the avalanche body. The flow regime determines which mechanism is dominant; plowing and abrasion require a dense, solid-like avalanche body, perhaps a plug flow, whereas impact erosion seems to be limited to more dilute flows (probably identifiable with the saltation layer). We anticipate a delicate interplay between erosion by fluidization and the avalanche density: the pressure gradient necessary for fluidization is produced only if the avalanching snow is sufficiently hard, dense and impermeable, but the fluidization process itself tends to dilute the avalanche front.

The erosion models presented here were not designed for direct use in any numerical code. Once the mechanisms are better understood, they have to be formulated in terms of the dynamical variables and parameters of the respective model. In view of the flow-regime dependence discussed above, advanced avalanche models explicitly recognizing different flow regimes (e.g. multi-layer models or models with dispersive pressure regulating the local density) are to be preferred over simple two-parameter models as platforms for realistic entrainment modules.

ACKNOWLEDGEMENTS

This work was funded through the Norwegian Geotechnical Institute's (NGI) SIP programs "Avalanche research" and "Offshore Geohazards" and through the European Union project SATSIE (Avalanche Studies and Model Validation in Europe), contract No. EVG1-CT2002-00059. We have received valuable information through enjoyable discussions with E. Adams, M. Barbolini, R. E. Brown, M. E. Eglit, H. Gubler, M. Schaer, J. Schweizer and B. Sovilla. We also wish to thank our colleagues of the avalanche group at NGI for their interest and discussions.

REFERENCES

- Abele, G. and A.J. Gow. 1975. Compressibility characteristics of undisturbed snow. *CRREL Res. Rep.* 336.
- Anderson, R. S. and P. K. Haff. 1991. Wind modification and bed response during saltation of sand in air. *Acta Mech.*, Supplementum 1. Aeolian Grain Transport. I: Mechanics, 21–52.
- Briukhanov, A.V. and 6 others. 1967. On some new approaches to the dynamics of snow avalanches. In Ōura, H., ed. *Physics of snow and ice. Vol. 1, Part 2*. Sapporo, Hokkaido University. Institute of Low Temperature Science, 1223–1241.
- Brugnot, G. and R. Pochat. 1981. Numerical simulation study of avalanches. *J. Glaciol.*, **27**(95), 77–88.
- Dufour, F., U. Gruber, D. Issler, M. Schaer, N. Dawes and M. Hiller. Unpublished. Grobauswertung der Lawineneignisse 1998/1999 im Grosslawinenversuchsgelände Vallée de la Sionne. Davos, Eidgenössisches Institut für Schnee- und Lawinenforschung. (Intern. Ber. 732.)
- Eglit, M. E. 1983. Some mathematical models of snow avalanches. In Shahinpoor, M., ed. *Advances in the mechanics and the flow of granular materials. Vol. 2*. Houston, TX, Gulf Publ. Co., 577–588.
- Eglit, M. E. 1998. Mathematical and physical modelling of powder snow avalanches in Russia. *Ann. Glaciol.*, **26**, 281–284.
- Fukushima, Y. and G. Parker. 1990. Numerical simulation of powder-snow avalanches. *J. Glaciol.*, **36**(123), 229–237.
- Gauer, P. 1995. A model of powder snow avalanches/Un modèle des avalanches poudreuses. In Sivardière, F., ed. *Les apports de la recherche scientifique à la sécurité neige, glace et avalanche/The contribution of scientific research to safety with snow, ice and avalanche. Actes de Colloque, Chamonix 30 mai–3 juin 1995*. Grenoble, Association Nationale pour l'Étude de la Neige et des Avalanches (ANENA), 55–61.
- Grigoryan, S. S. and A. V. Ostroumov. 1977. *Matematicheskaya model sklonovih processov lavinnogo tipa [The mathematical model for slope processes of avalanche type]*. Moscow, Institute for Mechanics, Moscow State University. [In Russian.]
- Hungr, O. 1995. A model for the runout analysis of rapid flow slides, debris flows and avalanches. *Can. Geotech. J.*, **32**(4), 610–623.
- Issler, D. 1998. Modelling of snow entrainment and deposition in powder-snow avalanches. *Ann. Glaciol.*, **26**, 253–258.
- Issler, D. 2003. Experimental information on the dynamics of dry-snow avalanches. In Hutter, K. and N. Kirchner, eds. *Dynamic response of granular and porous materials under large and catastrophic deformations*. Berlin, Springer, 109–160.
- Issler, D., P. Gauer and M. Barbolini. 2000. Continuum models of particle entrainment and deposition in snow drift and avalanche dynamics. In Bailean, R., ed. *Models of continuum mechanics in analysis and engineering*. Aachen–Maastricht, Shaker Verlag, 58–80.
- Issler, D., P. Gauer, M. Schaer and S. Keller. Unpublished. Staublwineneignisse im Winter 1995: Seewis (GR), Adalboden (BE) und Col du Pillon (VD). Davos, Eidgenössisches Institut für Schnee- und Lawinenforschung. (Intern. Ber. 694.)
- Iverson, R. M. 1997. The physics of debris flows. *Rev. Geophys.*, **35**(3), 245–296.
- Johnson, K.L. 2001. *Contact mechanics. Second edition*. Cambridge, Cambridge University Press.
- Maeno, N. and K. Nishimura. 1987. [Numerical computation of snow avalanche motion in a three-dimensional topography] *Low Temp. Sci., Ser. A*, **46**, 99–110. [In Japanese with English summary.]
- McElwaine, J. and K. Nishimura. 2001. Ping-pong ball avalanche experiments. *Ann. Glaciol.*, **32**, 241–250.
- Mears, A.I. 1980. A fragment-flow model of dry-snow avalanches. *J. Glaciol.*, **26**(94), 153–163.
- Mehta, A.J. 1991. Review notes on cohesive sediment erosion. In *Specialty Conference on Quantitative Approaches to Coastal Sediment Processes. Proceedings*. New York, American Society of Civil Engineers, 40–53.
- Parker, G., M. Garcia, Y. Fukushima and W. Yu. 1987. Experiments on turbidity currents over an erodible bed. *J. Hydraul. Res.*, **25**(1), 123–147.
- Partheniades, E. 1965. Erosion and deposition of cohesive soils. *ASCE J. Hydraul. Div.*, **91**(1), 105–139.
- Rabinowicz, E. 1995. *Friction and wear of materials. Second edition*. New York, etc., John Wiley and Sons.
- Rickerby, D. G. and N. H. Macmillan. 1980. On the oblique impact of a rigid sphere against a rigid-plastic solid. *Int. J. Mech. Sci.*, **22**(8), 491–494.
- Sailer, R., L. Rammer and P. Sampl. 2002. Recalculation of an artificially released avalanche with SAMOS and validation with measurements from a pulsed Doppler radar. *Nat. Hazards Earth System Sci.*, **2**(3/4), 211–216.
- Simon, A. and A. J. C. Collison. 2001. Pore-water pressure effects on the detachment of cohesive streambeds: seepage forces and matrix suction. *Earth Surf. Processes Landforms*, **26**(13), 1421–1442.
- Sommavilla, F. and B. Sovilla. 1998. The avalanche monitoring system of Mount Pizazzac. In Hestnes, E., ed. *25 Years of Snow Avalanche Research, Voss, 12–16 May 1998. Proceedings*. Oslo, Norwegian Geotechnical Institute, 268–273. (NGI Publication 203.)
- Sovilla, B. and P. Bartelt. 2002. Observations and modelling of snow avalanche entrainment. *Nat. Hazards Earth System Sci.*, **2**(3/4), 169–179.
- Sovilla, B., F. Sommariva and A. Tomaselli. 2001. Measurements of mass balance in dense snow avalanche events. *Ann. Glaciol.*, **32**, 230–236.
- Wilesa, M., K. L. Johnson and M. F. Ashby. 1975. Indentation of foamed plastics. *Int. J. Mech. Sci.*, **17**(7), 457–460.
- Zreik, D. A., R. G. Krishnappan, J. T. Germaine, O. S. Madsen and C. C. Ladd. 1998. Erosional and mechanical strengths of deposited cohesive sediments. *ASCE J. Hydraul. Eng.*, **124**(11), 1076–1085.